Pre-neuronal biomechanical filtering modulates and diversifies whole-hand tactile encoding

Neeli Tummala[1], Gregory Reardon[2], Bharat Dandu[1], Yitian Shao[3], Hannes P. Saal[4], Yon Visell[1,2,5,6*]

[1]Department of Electrical and Computer Engineering, University of California, Santa Barbara, Santa Barbara, CA 93106

[2]Department of Media Arts and Technology, University of California, Santa Barbara, Santa Barbara, CA 93106

[3]Department of Electrical and Computer Engineering, Technische Universität Dresden, Germany and Centre for Tactile Internet With Human-in-the-Loop (CeTI), Technische Universität Dresden, Germany

[4]Department of Psychology, University of Sheffield, Sheffield, United Kingdom S10 2TN

[5]Department of Biological Engineering, University of California, Santa Barbara, Santa Barbara, CA 93106

[6]Department of Mechanical Engineering, University of California, Santa Barbara, Santa Barbara, CA 93106

*To whom correspondence should be addressed; E-mail: yonvisell@ucsb.edu.

Abstract

When the hand touches a surface, the ensuing contact elicits skin oscillations that travel throughout the hand[1–4], driving responses in numerous exquisitely sensitive Pacinian corpuscle neurons (PCs)[5–8]. Although the tuning properties of individual PCs are well-documented[9–13], they have been characterized using stimuli applied adjacent to the receptor location. Such experiments are insensitive to the modulating influence of biomechanical filtering, which can significantly alter skin oscillations as they travel

through the hand's soft tissues[14–16]. Here, we used an integrated approach combining vibrometry imaging and computer simulation to characterize the effects of biomechanical filtering on evoked spiking activity in whole-hand PC populations. We observed complex distance- and frequency-dependent patterns of biomechanical transmission arising from the interplay of tissue mechanics and hand morphology. This source of modulation altered the response properties and spike timing of PCs, diversifying evoked activity in whole-hand PC populations. Together, these effects enhanced information encoding efficiency. These findings suggest that the biomechanics of the hand furnishes a pre-neuronal mechanism that facilitates efficient tactile processing.

The sense of touch is stimulated when we contact the environment with the skin. Tactile perceptual information is often regarded as originating with the responses of tactile sensory neurons terminating near the contact area. In humans and other animals, touch sensing also arises when the environment is felt indirectly through a probe, such as a tool, rodent whisker, or fingernail. Such probes are not innervated by sensory neurons. Instead, perceptual information is mediated by "internal contacts" that biomechanically couple the probe to other sensate tissues containing tactile sensory neurons[17]. Biomechanical couplings like those that mediate indirect touch are also integral to direct touch sensing with the skin due to intrinsic coupling within tissue. These couplings transmit mechanical signals to tissues not necessarily located near the region of contact, driving responses in widely distributed mechanoreceptors[1–4].

Indeed, recent findings show that haptic tasks, such as texture exploration[18], dexterous manipulation[19], and tool use[20], generate prominent skin oscillations that are transmitted across the hand. These oscillations convey information about the contact events that initiate them[14,16], which is reflected in responses of Pacinian corpuscle neurons (PCs) throughout the hand[5–8]. Thus, the intrinsic biomechanics of the hand transforms localized contact forces into spatially distributed skin oscillations that evoke responses in widespread sensory neurons. Previous studies also suggest that the skin oscillations driving PCs at distinct

hand locations are modified by filtering effects of biomechanics, including frequency- and location-dependent attenuation imparted by the heterogeneous soft tissues of the hand[5,14–16]. However, the implications for the response characteristics of PCs throughout the hand are unknown. Extant peripheral neural recordings reveal PC response behavior to be highly stereotyped, with highest sensitivity around $250\,\mathrm{Hz}$[9–13]. However, these recordings are obtained from sensory neurons adjacent to the site of skin contact and do not capture potential modulatory effects of biomechanical filtering on activity evoked in more distant PCs. Biomechanical filtering could substantially influence PC population encoding across the whole hand, but such effects and their implications for whole-hand tactile sensing have received little prior attention.

Here, we characterized the transmission of skin oscillations across the glabrous skin of several human hands (n = 7, P1-P7) and the neural spiking responses evoked in whole-hand PC populations. Mechanical impulses ($0.5\,\mathrm{ms}$ pulse width) were applied at four distinct contact locations and the evoked skin oscillations were recorded at 200 to 350 spatially-distributed locations via optical vibrometry (sample rate $20\,\mathrm{kHz}$, grid spacing $8\,\mathrm{mm}$, see Methods) (Fig. 1a). These impulse measurements characterized transmission across the hand within the frequency range relevant to PCs (20 - $800\,\mathrm{Hz}$) (Fig. 1b). The dispersive nature of biomechanical transmission altered both the temporal structure and frequency content of skin oscillations (Fig. 1b, d). As a consequence, we observed the pairwise temporal and spectral correlation of skin oscillations at different locations to decrease with increasing pairwise distance (Fig. 1c, d). Due to the linearity of skin biomechanics in the small signal regime, the impulse measurements accurately encoded the transmission of skin oscillations (Extended Data Fig. 1). This allowed us to compute the whole-hand patterns of skin oscillations that would be evoked by arbitrary tactile input waveforms via *in silico* experiments. We reconstructed the evoked skin oscillation patterns by convolving the waveform of interest with the ensemble of recorded impulses (see Methods). Using this technique, we computed skin oscillations evoked by tactile input signals including sinusoids, diharmonic signals, and bandpass filtered noise. This method preserved the modulatory effects of biomechanical filtering and the

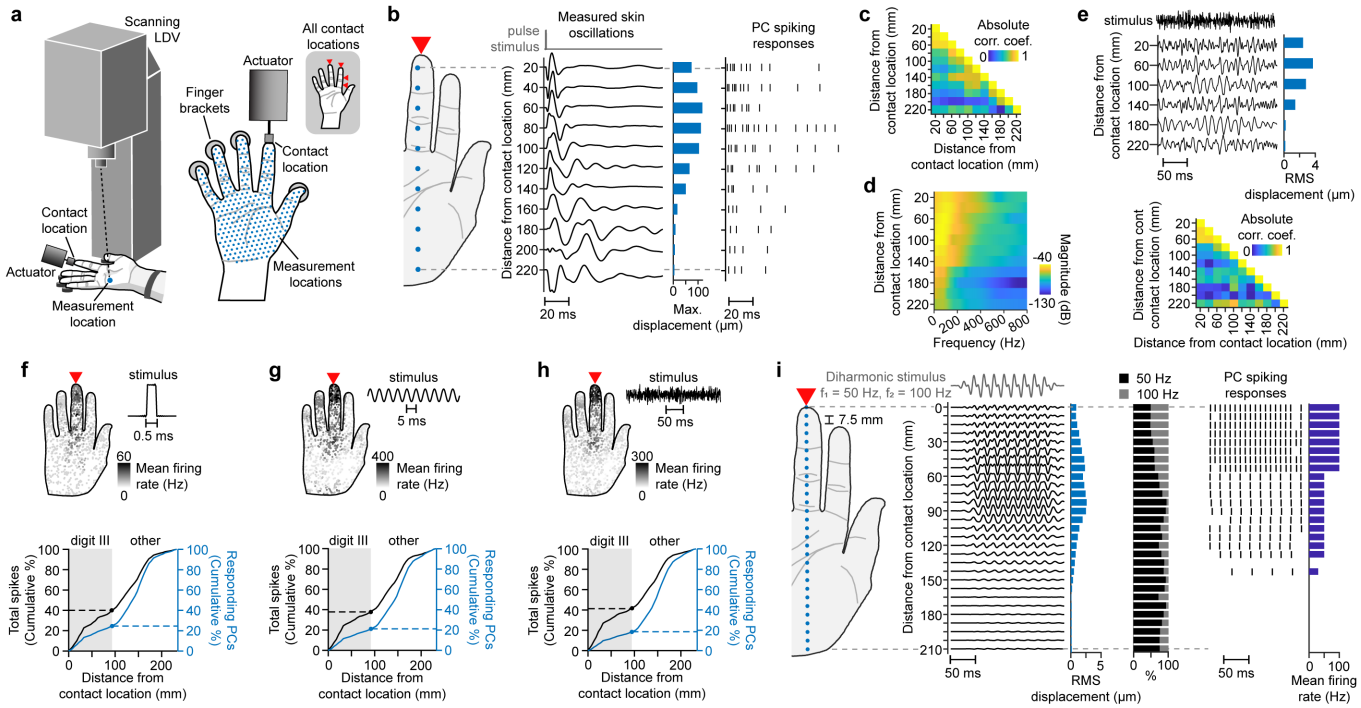

Fig. 1 | Biomechanically filtered skin oscillations drive PC responses throughout the hand. a, Scanning laser Doppler vibrometer (LDV) measurement setup. **b**, Left: vibrometry measurements of skin oscillations elicited by an impulse ($0.5\,\mathrm{ms}$ pulse width) applied at the digit III distal phalanx (DP). Right: PC spiking responses evoked by respective skin oscillations. **c**, Absolute Pearson correlation coefficients between skin oscillations shown in **b**. **d**, Magnitude of frequency spectrum of skin oscillations shown in **b**. **e**, Top: reconstructed skin oscillations elicited by bandpass noise stimulus (top trace, 50 - $800\,\mathrm{Hz}$) applied at the digit III DP. Bottom: Absolute Pearson correlation coefficients between skin oscillations at different distances from the contact location. **f**, Top: PC mean firing rates elicited by an impulse applied at the digit III DP ($15\,\mu\mathrm{m}$ max. peak-to-peak displacement across hand). Bottom: cumulative percent of total spikes (black) and responding PCs (blue) located within increasing distances from the contact location. Shaded region: results within digit III. **g**, As in **f**, for a $200\,\mathrm{Hz}$ sinusoidal stimulus ($15\,\mu\mathrm{m}$ max. peak-to-peak displacement across hand). **h**, As in **f**, for a bandpass noise stimulus (50 - $800\,\mathrm{Hz}$, $5\,\mu\mathrm{m}$ max. RMS displacement across hand). **i**, PC spiking responses (right) evoked by skin oscillations (middle) at selected locations (left, blue dots) elicited by a diharmonic stimulus ($f_1 = 50\,\mathrm{Hz}$, $f_2 = 100\,\mathrm{Hz}$) applied at the digit III DP. Light blue bars: RMS skin displacements; black and gray bars: percent of frequency magnitude spectrum composed of $50\,\mathrm{Hz}$ (black) or $100\,\mathrm{Hz}$ (gray) components; dark blue bars: PC mean firing rates. All plots show data from Participant 5 (P5).

resulting location-specific variations in the phase and amplitude of touch-elicited skin oscillations (Fig. 1e).

PC spiking responses are driven by deformations of the corpuscle that result from mechanical oscillations of surrounding tissues[13]. Thus, we sought to characterize the location-specific influences of biomechanical filtering on PC spiking responses. Current experimental techniques preclude the *in vivo* measurement of spiking responses of populations of PCs[21]. To overcome this limitation, we obtained whole-hand PC population spiking responses *in silico* by using computationally reconstructed skin oscillations to drive an ensemble of spiking neuron models that were fit to physiological data in prior research[22] (see Methods, Extended Data Fig. 2a), similar to the methodology applied in prior work investigating PC population responses during whole-hand touch events[23]. Each PC neuron model was driven by the skin oscillations at its respective location, and the spatial distribution of PCs across the hand was selected based on findings from a prior anatomical study[24]. We used this methodology to obtain spiking responses from whole-hand populations of PCs as evoked by arbitrary tactile inputs supplied at any of four contact locations on the hand.

Locally supplied stimuli evoked spiking activity in PCs located throughout the hand, consistent with predictions from theory and prior studies[3,5,7]. The majority of responding PCs and spiking activity originated in hand regions far removed from the contact location. This was observed for all stimulus types, including brief impulses (Fig. 1f), sinusoids (Fig. 1g, Extended Data Fig. 2c), and bandpass noise stimuli (Fig. 1h, Extended Data Fig. 2e). In each case, the effects of biomechanical filtering were reflected in the patterns of evoked spiking activity (Fig. 1b, i, Extended Data Fig. 2b, d). The temporal extent and patterns of spiking responses evoked by brief impulses varied in a location-specific manner, reflecting the complex interplay of PC spiking behavior and modulatory effects of biomechanics, including the dispersive propagation of oscillations in the skin (Fig. 1b). Further, PC responses exhibited characteristic entrainment behavior (phase-locking to the oscillations of periodic stimuli) that reflected the effects of biomechanical filtering. When a diharmonic stimulus was supplied at the fingertip, PCs located near the contact location ($<60\,\mathrm{mm}$) entrained to the high frequency ($100\,\mathrm{Hz}$) signal component, while more distant PCs entrained to the lower frequency ($50\,\mathrm{Hz}$) component (Fig. 1i). This change in entrainment behavior with distance from

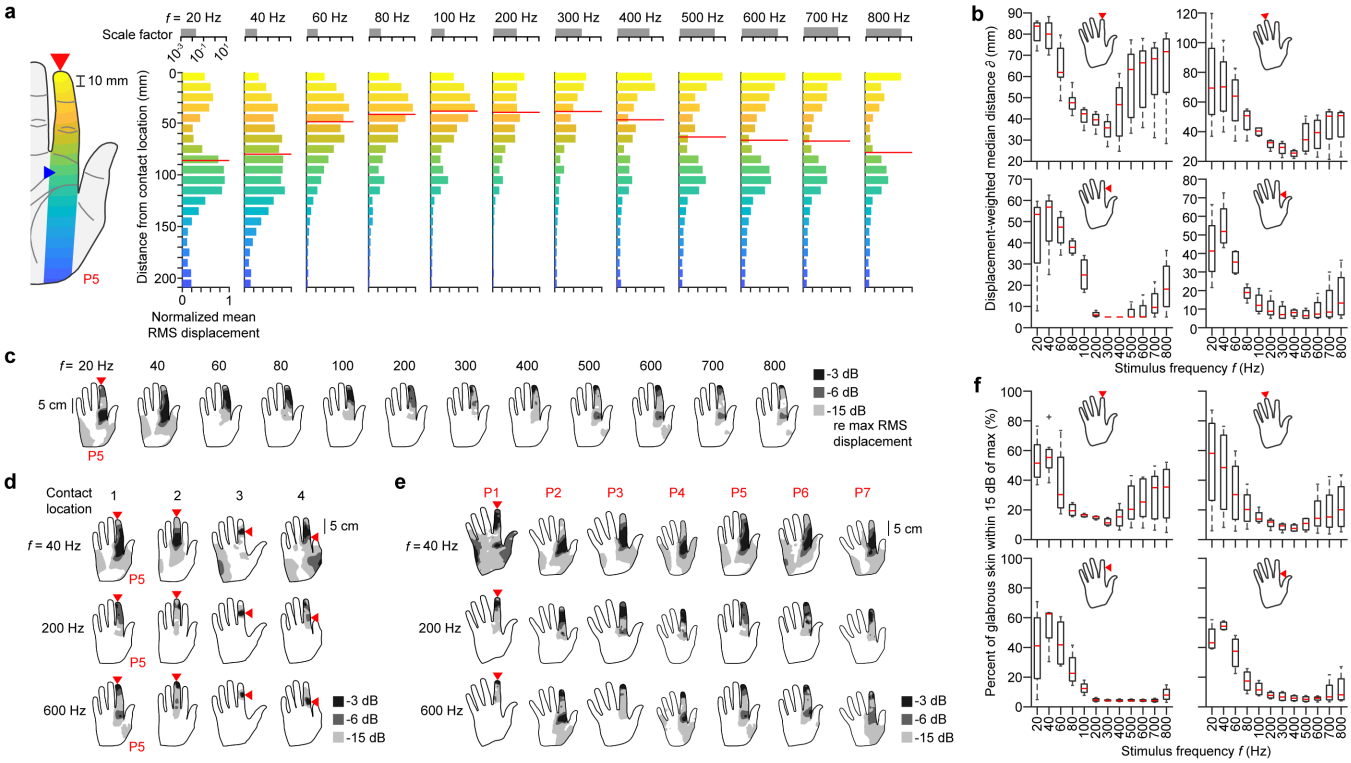

Fig. 2 | Biomechanical filtering in the hand is frequency- and location-dependent. **a**, Normalized distribution of mean root mean square (RMS) skin displacement within 10 mm-wide bands at increasing distances from the contact location elicited by sinusoidal stimuli of various frequencies (20 - 800 Hz). At each frequency, skin displacements were multiplied by a scale factor (top, gray bars) to ensure that the maximum peak-to-peak skin displacement across the hand was 50 µm. Red lines: median transmission distance of RMS displacement distributions; red arrow: contact location; blue arrow: metacarpophalangeal (MCP) joint region of digit II; red text: participant number. **b**, Median transmission distance of RMS skin displacement distributions across frequency, calculated as in **a**. Red arrows: contact location; red lines: median; lower box limits: 25th percentile; upper box limits: 75th percentile; whiskers: range of data within 2.7 times the standard deviation; + symbols: outliers across all participants. **c**, Regions of glabrous skin within 3 (dark gray), 6 (gray), and 15 dB (light gray) of the maximum RMS skin displacement across the hand elicited by sinusoidal stimuli of various frequencies (20 - 800 Hz). Red arrow: contact location; red text: participant number. **d, e**, As in **c**, for other contact locations and participants. **f**, Percent of glabrous skin covered by 15 dB regions at each frequency. Plots can be read as in **b**.

the contact location reflected the attenuation of the higher frequency component of skin oscillation due to frequency-dependent modulatory effects imparted by biomechanics (Fig. 1i, black and gray bars).

The frequency-dependence of biomechanical filtering arises from the viscoelastic characteristics of

soft tissues[15], as well as the skeletal structure of the hand. To more systematically characterize these effects, we analyzed skin oscillations evoked by sinusoidal stimuli of different frequencies, with amplitudes normalized to account for the relative mobility of the skin at different frequencies (see Methods). Skin oscillations elicited by sinusoidal stimuli exhibited complex frequency-dependent amplitude patterns that displayed non-monotonic decay with distance (Fig. 2a, Extended Data Fig. 3). We characterized variations in the overall attenuation of skin oscillations as a function of frequency by computing the median transmission distance. We observed low- ($<80\,\mathrm{Hz}$) and high-frequency ($>400\,\mathrm{Hz}$) components to reach substantial distances extending beyond the stimulated digit, while intermediate frequency components were predominantly confined within the digit. Findings were consistent across all hands and stimulus locations (Fig. 2b).

The complex, frequency-dependent patterns of transmission of skin oscillations across the hand surface were also influenced by the heterogeneous morphology and skeletal structure of the hand (Fig. 2c-f, Extended Data Fig. 4). Transmission was notably enhanced in regions near the metacarpophalangeal (MCP) joint of the stimulated digit, where oscillation amplitudes were within $6\,\mathrm{dB}$ of the maximum RMS displacement across the hand at both low and high frequencies ($<100\,\mathrm{Hz}$, $>400\,\mathrm{Hz}$) (Fig. 2c). Transmission was also enhanced to the lateral and contralateral extensions of the palmar surface (thenar and hypothenar eminences), especially at low frequencies ($<80\,\mathrm{Hz}$). These low frequencies produced prominent oscillations (within $15\,\mathrm{dB}$ of maximum) over a significant proportion of the hand surface (mean $43\,\%$). In contrast, higher frequencies between 100 and $400\,\mathrm{Hz}$ evoked skin oscillations over a significantly smaller proportion of the hand surface (mean $10.5\,\%$) (Fig. 2f). We obtained similar findings for different contact locations (Fig. 2d), with the notable exception that high-frequency stimuli ($>400\,\mathrm{Hz}$) delivered orthogonal to the axis of the digit evoked skin oscillations spanning a smaller area than was excited in other contact conditions. These findings were generally consistent across participants (Fig. 2e).

To quantify the effects of biomechanical filtering on PC frequency response characteristics, we next studied whole-hand PC spiking activity evoked by sinusoidal stimuli supplied at each of the four contact

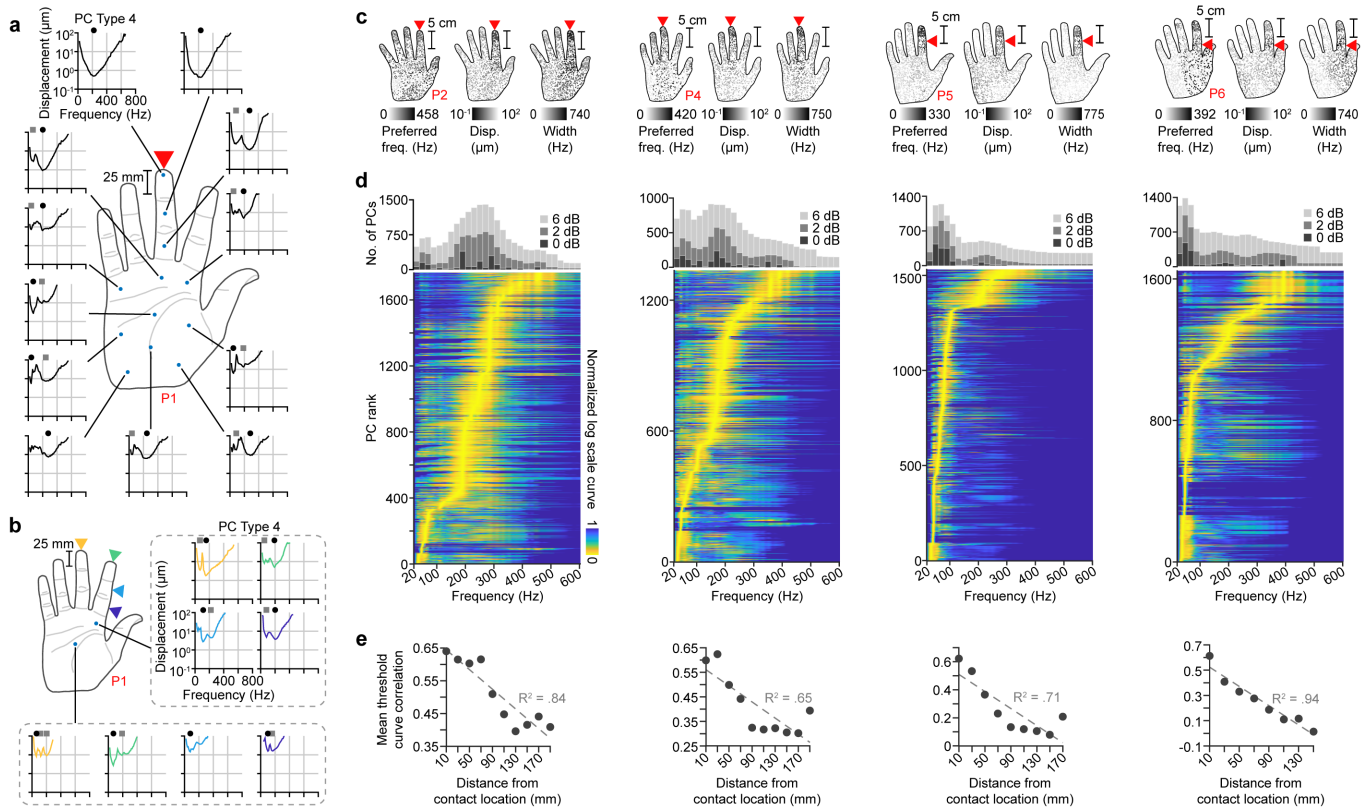

Fig. 3 | Biomechanical filtering diversifies PC response characteristics. a, Entrainment threshold curves of PCs at selected locations on the hand. Red arrow: contact location; red text: participant number; blue dots: PC locations; black circles above curves: global minimum, gray squares above curves: other local minima (prominence > 0.25). Shown for PC neuron model type 4. **b**, Entrainment threshold curves of PCs at two locations on the hand for each of 4 contact locations. Colored arrows and lines: contact locations; red text: participant number; black circles above curves: global minimum; gray squares above curves: other local minima (prominence > 0.25). Shown for PC neuron model type 4. **c**, Preferred frequency (left), minimum curve value (middle), and curve width (right) for each PC in the hand. Red arrow: contact location; red text: participant number. **d**, Entrainment threshold curves for all PCs in the hand rank ordered by preferred frequency. Participants and contact locations correspond to **c**. Histograms: number of PCs at each frequency with entrainment threshold curve values within 0 (light gray), 2 (medium gray), and $6\,\mathrm{dB}$ (dark gray) of the global minimum. **e**, Mean Pearson correlation coefficient between all pairs of entrainment threshold curves of PCs located within $10\,\mathrm{mm}$ of the contact location and those of PCs located within $20\,\mathrm{mm}$-wide bands at increasing distances from the contact location. X-axis labels denote the center distance of each band. Gray dotted lines: linear fits; gray text: R^2 values; red text: participant number. Participants and contact locations correspond to those in **c** and **d**.

locations. We quantified the frequency-dependent sensitivity of PCs by determining entrainment threshold curves that represent the minimum displacement required to evoke entrainment at each frequency (see Methods). PCs located near the contact location exhibited U-shaped entrainment threshold curves with preferred (most sensitive) frequencies between 200 and $300\,\mathrm{Hz}$ (Fig. 4a, Extended Data Fig. 5a). This result is consistent with prior *in vivo* studies of individual PCs performed by applying the stimulus at the location of the PC[9–13]. In contrast, entrainment threshold curves for PCs away from the contact location varied greatly and exhibited multiple prominent minima due to the location-specific filtering of skin oscillations (Fig. 4a, Extended Data Fig. 5b, c). Moreover, the frequency sensitivity of a given PC varied greatly depending on the contact location (Fig. 4b).

We next examined the diversity in PC frequency response characteristics across whole-hand PC populations by rank ordering entrainment threshold curves by preferred frequency (Fig. 4c, d, Extended Data Fig. 6). Across the population, PCs exhibited preferred frequencies that ranged widely from 25 to $500\,\mathrm{Hz}$. The preferred frequencies of PCs located near the contact location were consistent with values obtained in prior studies of individual PCs (200 - $300\,\mathrm{Hz}$), but PCs further away from the contact location had a wider range of frequency sensitivities (Extended Data Fig. 7). Strikingly, across all participants and contact locations, a substantial proportion of PCs in a population (mean $42\,\%$) preferred frequencies below $100\,\mathrm{Hz}$. In addition, PCs at greater distances from the contact location were generally less sensitive with elevated thresholds and exhibited more narrowly tuned curves.

However, threshold curves had complex shapes not adequately summarized by preferred frequency or curve width and varied greatly with location. To characterize distance-dependent variations in the entrainment curves, we calculated pairwise correlations between threshold curves of PCs at the contact location and those at progressively greater distances across the hand (see Methods, Fig. 4e, Extended Data Fig. 8). For all participants and contact locations, the mean pairwise correlation decreased with increasing distance from the contact location (0.026 - 0.076 per $20\,\mathrm{mm}$, $R^2 = 0.58$ - 0.94). These findings demonstrate that pre-neuronal biomechanical filtering diversifies frequency response characteristics in

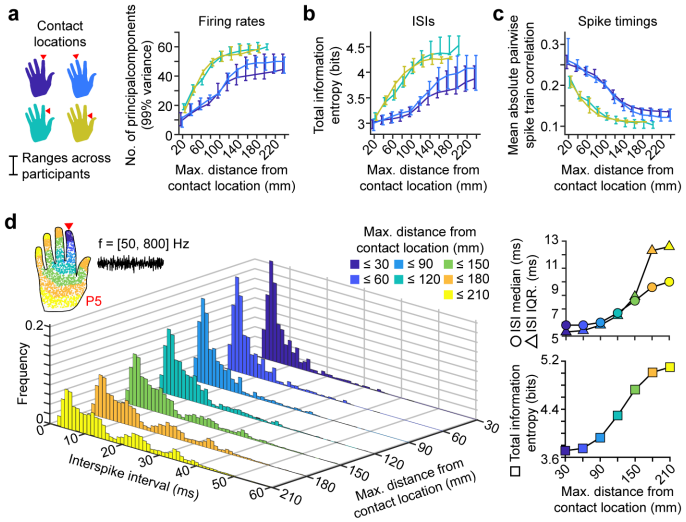

Fig. 4 | Biomechanical filtering diversifies PC spiking activity. **a**, Number of principal components explaining $99\,\%$ of the variance in firing rates of PCs located within increasing distances from the contact location. Vertical bars: ranges across participants; red arrows and line color: contact location. **b**, Total information entropy of interspike interval (ISI) histograms (bin width $1\,\mathrm{ms}$) constructed from PCs located within increasing distances from the contact location. Plot can be read as in **a**. **c**, Mean absolute spike train correlation between all pairs of PCs located within increasing distances from the contact location. Spike trains were binned with a bin width of $1\,\mathrm{ms}$. Plot can be read as in **a**. **d**, Left: Histograms comprising ISIs from PCs located within increasing distances from the contact location (hand inset) in response to a bandpass noise stimulus (50- $800\,\mathrm{Hz}$, $5\,\mu\mathrm{m}$ max. RMS displacement across hand, $175\,\mathrm{ms}$ duration) applied at the digit II DP of P5. Right: median (circles), interquartile range (triangles), and total information entropy (squares) of the ISI histograms shown to the left.

whole-hand PC populations.

We next asked whether this diversification enhanced information encoding in PC population spiking responses, particularly for the majority of responding PCs that are distant from the contact location. To answer this question, we characterized the dimensionality and information content of PC population spiking activity as a function of distance from the contact location (see Methods). Informed by prior research[25,26], we analyzed PC activity evoked by a diverse set of tactile stimuli, including sinusoidal, diharmonic, and bandpass noise signals, that spanned the range of everyday tactile experiences. First, we characterized the latent dimensionality of PC firing rates in subpopulations of PCs with increasing maximum distances from the contact stimulus. Dimensionality, calculated as the number of principal components needed to capture

$99\,\%$ of the variance, was 2 to 4 times higher at distances of 80 - $140\,\mathrm{mm}$ from the contact location than it was at closer distances of $< 20\,\mathrm{mm}$ (Fig. 4a). These findings were consistent across all participants and contact locations. Thus, evoked activity in PCs at increasing distances from the contact location captured progressively more variance, highlighting the facilitative role of biomechanical filtering in PC population encoding.

We next characterized PC spike timing by computing interspike interval (ISI) histograms evoked by each stimulus type. In all cases, ISIs were larger and more broadly distributed with increasing distance from the contact location (Fig. 4d, Extended Data Fig. 9). As a consequence, information encoded by the ISI histograms (Shannon entropy) increased monotonically with distance by a factor of 1.15 to 1.5 before plateauing at 100 - $180\,\mathrm{mm}$ from the contact location (Fig. 4b). The findings were robust to variations in ISI histogram bin widths (Extended Data Fig. 10). Consistent with these findings, our analyses of spike train correlations revealed the spiking activity of PCs at increasing distances to be progressively less correlated with the activity of PCs near the contact location (Fig. 4c, Extended Data Fig. 11). Together, these findings indicate that biomechanical filtering diversifies PC spiking activity while also preserving a degree of response redundancy among PCs.

Our study combines high-resolution vibrometry measurements of whole-hand biomechanical transmission with neural simulations using extensively validated neuron models[22] to elucidate the pre-neuronal role of biomechanical filtering on diversifying tactile encoding within the PC system. Our findings demonstrate that PC population responses across the hand are significantly modulated by biomechanical filtering and therefore differ markedly from responses of individual PCs located near the contact location. Because PCs at substantial distances are more numerous than those adjacent to the contact location, the responses of more distant PCs represent a dominant proportion of the population response and can be expected to affect downstream tactile processing and ultimately perception.

The frequency-dependent patterns of biomechanical transmission and filtering we observed are generally consistent with prior characterizations of mechanical propagation in individual fingers[14,15,27],

taking into account likely differences in contact conditions. Here, we present whole-hand measurements at significantly greater spatiotemporal resolution than those used in prior studies. This made it possible to resolve the effects of biomechanical transmission and filtering throughout the hand, including pronounced differences between evoked signals disseminated to the fingers and palm, non-monotonic decay of oscillation amplitude with distance, and contact location dependent variations in filtering across hand areas.

The observed effects of biomechanical filtering in diversifying frequency response characteristics across PC populations are somewhat analogous to the frequency-place transform effected by the mammalian cochlea[28,29] but instead facilitated by the morphology and biomechanics of the hand. Despite the observed complexities of biomechanical transmission in the hand, several core characteristics of the evoked spatiotemporal patterns of skin oscillation were conserved across multiple hands and stimulus locations. These include the frequency-dependent patterns of oscillation amplitude with distance, increased transmission distances at low ($<100\,\mathrm{Hz}$) and high ($>400\,\mathrm{Hz}$) frequencies, and the amplification of transmission near the MCP joint driven by the hand's anatomy. These findings demonstrate how biomechanical filtering generates a spatial and spectral structure that the brain could learn and exploit, similar to hypotheses for efficient encoding of whole-hand touch events[16], object slippage[30], and tool use[20].

Our findings may also shed light on a number of peculiar aspects of PC innervation of the hand. Despite their stereotyped response properties and large receptive fields, which span most of the hand, PCs in the glabrous skin number in the hundreds or more[31–33]. Considered in isolation, these characteristics would imply tremendous response redundancy, which would be at odds with encoding efficiency hypotheses[34–36]. However, our results demonstrate that biomechanical filtering diversifies PC response characteristics, thereby reducing PC population response redundancy and enhancing encoding efficiency. Furthermore, prominent clusters of PCs are observed near the MCP joints in human hands[32,33]. Near those locations, we observed consistently elevated oscillation amplitudes, suggesting that PCs may be preferentially located in regions of the hand where biomechanical transmission is facilitated.

More generally, the pronounced effect of biomechanics on the evoked PC responses exemplifies how pre-neuronal mechanisms can play a crucial role in sensory processing. Analogous conclusions have been drawn in studies of the rodent vibrissal system, where the mechanics of the whiskers are instrumental to tactile neural coding[37,38]. Moreover, a recent study based on recordings of PC responses in freely moving mice revealed prominent effects of biomechanical transmission and substantial diversity in PC response characteristics broadly consistent with our findings[39].

Finally, there is ample prior evidence for the perceptual relevance of touch-elicited skin oscillations away from the contact location. For example, textures can be discriminated even under anesthesia of the hand[6], mediated by skin oscillations reaching the wrist[3]. Furthermore, the spatial extent of evoked skin oscillations depends on stimulation frequency, an effect that can be exploited to design tactile inputs that evoke percepts with varying spatial extent[15]. Accounting for the diverse response characteristics of PC populations may shed light on their involvement in perception and behavior in other settings. For example, the perceived intensity of vibrations depends strongly on stimulation frequency[40,41], but this dependence does not agree with predictions derived based on responses of individual PCs[25]. Moreover, proposed models for the perception of polyharmonic stimuli assume the existence of neural subpopulations that vary in frequency selectivity[42], which contrasts with the broad and stereotyped frequency tuning exhibited by isolated PCs. The prominent influence of biomechanics in the dissemination and filtering of tactile signals throughout the hand and the resulting modulatory effects on neural population responses suggest that these factors have important implications for subsequent tactile processing and ultimately perception.

References

1. Moore, T. J. A Survey of the Mechanical Characteristics of Skin and Tissue in Response to Vibratory Stimulation. *IEEE Transactions on Man-Machine Systems* **11,** 79–84 (1970).
2. Pubols, B. H. Effect of Mechanical Stimulus Spread across Glabrous Skin of Raccoon and Squirrel Monkey Hand on Tactile Primary Afferent Fiber Discharge. *Somatosensory Research* **4,** 273–308 (1987).
3. Delhaye, B., Hayward, V., Lefèvre, P. & Thonnard, J.-L. Texture-induced vibrations in the forearm during tactile exploration. *Frontiers in Behavioral Neuroscience* **6** (2012).
4. Shao, Y., Hayward, V. & Visell, Y. Spatial patterns of cutaneous vibration during whole-hand haptic interactions. *Proceedings of the National Academy of Sciences* **113,** 4188–4193 (2016).
5. Manfredi, L. R. *et al.* The Effect of Surface Wave Propagation on Neural Responses to Vibration in Primate Glabrous Skin. *PLOS ONE* **7,** e31203 (2012).
6. Libouton, X., Barbier, O., Berger, Y., Plaghki, L. & Thonnard, J.-L. Tactile roughness discrimination of the finger pad relies primarily on vibration sensitive afferents not necessarily located in the hand. *Behavioural Brain Research* **229,** 273–279 (2012).
7. Andrews, J. W., Adams, M. J. & Montenegro-Johnson, T. D. A universal scaling law of mammalian touch. *Science Advances* **6,** eabb6912 (2020).
8. Corniani, G., Casal, M. A., Panzeri, S. & Saal, H. P. Population coding strategies in human tactile afferents. *PLOS Computational Biology* **18,** e1010763 (2022).
9. Sato, M. Response of Pacinian corpuscles to sinusoidal vibration. *The Journal of Physiology* **159,** 391–409 (1961).
10. Talbot, W. H., Darian-Smith, I., Kornhuber, H. H. & Mountcastle, V. B. The sense of flutter-vibration: comparison of the human capacity with response patterns of mechanoreceptive afferents from the monkey hand. *Journal of Neurophysiology* **31,** 301–334 (1968).
11. Johansson, R. S., Landström, U. & Lundström, R. Responses of mechanoreceptive afferent units in the glabrous skin of the human hand to sinusoidal skin displacements. *Brain Research* **244,** 17–25 (1982).
12. Bolanowski, S. J. & Zwislocki, J. J. Intensity and frequency characteristics of pacinian corpuscles. I. Action potentials. *Journal of Neurophysiology* **51,** 793–811 (1984).
13. Bell, J., Bolanowski, S. & Holmes, M. H. The structure and function of pacinian corpuscles: A review. *Progress in Neurobiology* **42,** 79–128 (1994).
14. Manfredi, L. R. *et al.* Natural scenes in tactile texture. *Journal of Neurophysiology* **111,** 1792–1802 (2014).
15. Dandu, B., Shao, Y. & Visell, Y. Rendering Spatiotemporal Haptic Effects Via the Physics of Waves in the Skin. *IEEE Transactions on Haptics* **14,** 347–358 (2020).

16. Shao, Y., Hayward, V. & Visell, Y. Compression of dynamic tactile information in the human hand. *Science Advances* **6** (2020).

17. Gibson, J. *The senses considered as perceptual systems* (Houghton Mifflin, Oxford, England, 1966).

18. BensmaÏa, S. J. & Hollins, M. The vibrations of texture. *Somatosensory & Motor Research* **20,** 33–43 (2003).

19. Johansson, R. S. & Flanagan, J. R. Coding and use of tactile signals from the fingertips in object manipulation tasks. *Nature Reviews Neuroscience* **10,** 345–359 (2009).

20. Miller, L. E. *et al.* Sensing with tools extends somatosensory processing beyond the body. *Nature* **561,** 239–242 (2018).

21. Deflorio, D., Di Luca, M. & Wing, A. M. Skin and Mechanoreceptor Contribution to Tactile Input for Perception: A Review of Simulation Models. *Frontiers in Human Neuroscience* **16** (2022).

22. Saal, H. P., Delhaye, B. P., Rayhaun, B. C. & Bensmaia, S. J. Simulating tactile signals from the whole hand with millisecond precision. *Proceedings of the National Academy of Sciences* **114,** E5693–E5702 (2017).

23. Tummala, N., Shao, Y. & Visell, Y. *Spatiotemporal organization of touch information in tactile neuron population responses* in *Proceedings of the IEEE World Haptics Conference (WHC)* (2023).

24. Johansson, R. S. & Vallbo, A. B. Tactile sensibility in the human hand: relative and absolute densities of four types of mechanoreceptive units in glabrous skin. *The Journal of Physiology* **286,** 283–300 (1979).

25. Muniak, M. A., Ray, S., Hsiao, S. S., Dammann, J. F. & Bensmaia, S. J. The Neural Coding of Stimulus Intensity: Linking the Population Response of Mechanoreceptive Afferents with Psychophysical Behavior. *Journal of Neuroscience* **27,** 11687–11699 (2007).

26. Mackevicius, E. L., Best, M. D., Saal, H. P. & Bensmaia, S. J. Millisecond Precision Spike Timing Shapes Tactile Perception. *The Journal of Neuroscience* **32,** 15309 (2012).

27. Wiertlewski, M. & Hayward, V. Mechanical behavior of the fingertip in the range of frequencies and displacements relevant to touch. *Journal of Biomechanics* **45,** 1869–1874 (2012).

28. V. Békésy, G. Human Skin Perception of Traveling Waves Similar to Those on the Cochlea. *The Journal of the Acoustical Society of America* **27,** 830–841 (1955).

29. Saal, H., Wang, X. & Bensmaia, S. Importance of spike timing in touch: an analogy with hearing? *Current Opinion in Neurobiology* **40,** 142–149 (2016).

30. Willemet, L., Huloux, N. & Wiertlewski, M. Efficient tactile encoding of object slippage. *Scientific Reports* **12,** 13192 (2022).

31. Corniani, G. & Saal, H. P. Tactile innervation densities across the whole body. *Journal of Neurophysiology* **124,** 1229–1240 (2020).

32. Stark, B., Carlstedt, T., Hallin, R. G. & Risling, M. Distribution of Human Pacinian Corpuscles in the Hand: A cadaver study. *Journal of Hand Surgery* **23,** 370–372 (1998).

33. Germann, C., Sutter, R. & Nanz, D. Novel observations of Pacinian corpuscle distribution in the hands and feet based on high-resolution 7-T MRI in healthy volunteers. *Skeletal Radiology* **50,** 1249–1255 (2021).

34. Barlow, H. B. in *Sensory Communication* (ed Rosenblith, W. A.) (The MIT Press, 1961).

35. Field, D. J. Relations between the statistics of natural images and the response properties of cortical cells. *JOSA A* **4,** 2379–2394 (1987).

36. Atick, J. J. Could information theory provide an ecological theory of sensory processing? *Network: Computation in Neural Systems* **22,** 4–44 (2011).

37. Bagdasarian, K. *et al.* Pre-neuronal morphological processing of object location by individual whiskers. *Nat. Neurosci.* (2013).

38. Ding, Y. & Vlasov, Y. Pre-neuronal processing of haptic sensory cues via dispersive high-frequency vibrational modes. *Sci. Rep.* **13,** 14370 (2023).

39. Turecek, J. & Ginty, D. D. Coding of self and environment by Pacinian neurons in freely moving animals, 2023.09.11.557225 (2023).

40. Stevens, S. S. Tactile vibration: Change of exponent with frequency. *Atten. Percept. Psychophys.* **3,** 223–228 (1968).

41. Verrillo, R. T., Fraioli, A. J. & Smith, R. L. Sensation magnitude of vibrotactile stimuli. *Atten. Percept. Psychophys.* **6,** 366–372 (1969).

42. Bensmaia, S., Hollins, M. & Yau, J. Vibrotactile intensity and frequency information in the Pacinian system: A psychophysical model. *Perception & Psychophysics* **67,** 828–841 (2005).

Methods

In vivo optical vibrometry

Mechanical oscillations across the volar hand surface were imaged via scanning laser Doppler vibrometer (SLDV; model PSV-500, Polytec, Inc., Irvine, CA; sample frequency $20\,\mathrm{kHz}$) fastened to a pneumatically isolated table. During each recording, the hand was fixated on the table in an open, palm-up posture via custom fit 3D printed supports that were fastened to the table and adhered to the fingernails of all but the stimulated digit (Fig. 1). Participants ($n = 7$) were 20 to 45 years of age. They were seated in a reclined chair with the arm relaxed and supported by a foam armrest and Velcro straps. All subjects gave their informed, written consent prior to the data collection. The study was approved by the Human Subjects Committee of the University of California, Santa Barbara.

The SLDV imaged spatially and temporally resolved skin oscillations at sampling locations distributed on a uniform grid extending across the entire volar hand surface (grid spacing $8\,\mathrm{mm}$, 200 - 350 locations). The sampling grid exceeded the Nyquist criterion threshold for frequencies in the tactile range (20 - $100\,\mathrm{mm}$ spatial wavelengths)[16]. Oscillations were imaged in the normal direction to the skin surface. Prior vibrometry measurements have demonstrated that most of the energy in evoked skin oscillations is concentrated in oscillations normal to the skin surface[15] and that stress in the normal direction is highly predictive of PC spiking responses[22].

All data were captured from the right hands of participants. Hand lengths ranged from 18 to $21.6\,\mathrm{cm}$ as measured from the tip of digit III to the bottom of the hand at the middle of the wrist. Each hand was positioned $360\,\mathrm{mm}$ below the SLDV aperture. This ensured that the measurements captured at least $95\,\%$ of the signal variance at all measurement locations. Hand shape and 2D spatial coordinates of all measurement locations were captured via the integrated SLDV geometry processor and camera. Measurements were interpolated to obtain skin oscillations at other locations on the 2D hand surface (see Supplementary Methods).

Measured skin oscillations were evoked by mechanical impulses (rectangular pulse, duration $0.5\,\mathrm{ms}$) applied at each of four contact locations, described below. Measurements were synchronized to the stimulus onset. Each measurement was obtained as the median of 10 captures and bandpass filtered to the tactile frequency range (20 - $1000\,\mathrm{Hz}$). Numerical integration was employed to obtain skin displacement from velocity. Stimuli were delivered via an electrodynamic actuator (Type 4810, Brüel & Kjær) driven with a laboratory amplifier (PA-138, Labworks). The actuator terminated in a plastic probe ($7{\times}7\,\mathrm{mm}$ contact surface) that was adhesively attached to the skin at the stimulus contact location. The actuator and probe were configured to avoid obstructing the optical path used for the SLDV measurements.

Stimuli were applied at each of four different contact locations registered to the respective hand anatomy: the distal phalanx (DP) of digit II along the axis of the finger (Contact Location 1, n = 7 participants), the DP of digit III along the axis of the finger (Contact Location 2, n = 4), the intermediate phalanx (IP) of digit II perpendicular to the axis of the finger (Contact Location 3, n = 4), and the proximal phalanx (PP) of digit II perpendicular to the axis of the finger (Contact Location 4, n = 4). These measurements took approximately 10 minutes per contact condition, per participant.

Computing skin oscillations evoked by arbitrary stimuli

Theory and experimental findings[43] indicate that biomechanical transmission in the hand is linear for stimulus magnitudes in the regime employed here. Consequently, the propagation of evoked skin oscillations is linear and may be mathematically described by a wave equation of the form $L\,u(\mathbf{x},t) = 0$, where L is a linear operator encoding transport in the respective hand and configuration, $\mathbf{x}$ is a skin location, t is time, and $u(\mathbf{x},t)$ is the evoked skin oscillations. From linear systems theory, an arbitrary force stimulus $F(t)$ applied to the skin at location $\mathbf{x}_0$ evokes oscillations $u(\mathbf{x},t)$ given by

$$u(\mathbf{x},t) = g_{\mathbf{x}_0}(\mathbf{x},t) * F(t) \tag{1}$$

where $*$ denotes convolution in time and $g_{\mathbf{x}_0}(\mathbf{x},t)$ is the empirical Green's function encoding the excitation of skin oscillations evoked by an idealized unit impulse force applied at $\mathbf{x}_0$. We determined the empirical

Green's functions for each hand and contact location $\mathbf{x}_0$ using the impulse-driven skin oscillation measurements described above. The skin oscillations evoked by arbitrary stimuli $F(t)$ were determined numerically, through the application of Equation 1. To confirm the accuracy of this method, we compared the results obtained for sinusoidal stimuli $F(t)$ over a large range of frequencies (20 - 640 Hz). Apart from the stimulus waveform, the measurement procedure was otherwise identical to the one described above. Consistent with linear systems theory, we found that the numerically determined oscillations closely approximated the actual measurements (Extended Data Figure 1). We thus employed a numerical methodology to determine skin oscillations evoked by arbitrary stimuli in the remainder of our experiments.

Stimuli

We analyzed skin oscillations $u(\mathbf{x}, t)$ evoked by sinusoidal, diharmonic, and bandpass noise stimulus waveforms, $F(t)$. For sinusoidal stimuli, $F(t) = A \sin(2\pi f t)$, where f is frequency and A is an amplitude scaling factor. For diharmonic stimuli, $F(t) = A_1 \sin(2\pi f_1 t) + A_2 \sin(2\pi f_2 t)$, with independent scaling factors A_1 and A_2. The phase difference between frequency components was always 0. Skin oscillations elicited by diharmonic stimuli were obtained via superposition, $u(\mathbf{x}, t) = u_1(\mathbf{x}, t) + u_2(\mathbf{x}, t)$, where u_1 and u_2 are the sinusoidal components. Bandpass noise stimuli were synthesized using a spectral Gaussian white noise algorithm[44] followed by bandpass filtering to the desired frequency range. Each bandpass noise stimulus was generated from the same Gaussian white noise trace, scaled by a factor A.

The amplitudes of sinusoidal stimuli were selected to ensure that the maximum peak-to-peak displacement of skin oscillations across all hand locations was matched between stimuli. The scale values A were thus computed using

$$D_{pp} = A \max_{\mathbf{x}} \left\{ \max_t \{u(\mathbf{x}, t)\} - \min_t \{u(\mathbf{x}, t)\} \right\}, \tag{2}$$

where D_{pp} is the desired maximum peak-to-peak displacement across the hand. The same method was used

to independently select the amplitudes A_1 and A_2 of each sinusoidal component of the diharmonic stimuli. A similar approach was used for bandpass noise stimuli, but due to their stochastic nature, the maximum RMS displacement of skin oscillations across hand locations was controlled. The scale values A were thus computed using

$$D_{RMS} = A \max_{\mathbf{x}} \{u_{RMS}(\mathbf{x})\}, \tag{3}$$

where D_{RMS} is the desired maximum RMS displacement across the hand and $u_{RMS}(\mathbf{x})$ is the RMS displacement at location $\mathbf{x}$.

Whole-hand neural simulations

PC spiking responses were obtained by using the skin oscillation vibrometry data to drive biologically plausible spiking neuron models (Extended Data Fig. 2a). The individual PC neuron models were extracted from the simulation package (Touchsim, Python) associated with a prior research study in which the PC neuron model parameters for each of four PC types were fit to a large dataset of macaque electrophysiology recordings[22,25]. Each PC neuron model type varies slightly in response properties (Extended Data Fig. 5a). The PC neuron models supply a dynamic, nonlinear mapping from skin displacement to spiking output and accurately reproduce experimentally identified response characteristics of PCs, including response thresholds that vary across several orders of magnitude over tactile frequency range (1 - $1000\,\mathrm{Hz}$)[10,12] and frequency-dependent thresholds for entrainment[9,11,13]. We selected the range of stimulus amplitudes used in our experiments to fall within the range over which the PC models were validated.

Whole-hand PC populations were assembled by sampling a random distribution weighted by densities that were reported in prior studies: $25/\mathrm{cm}^2$ in the distal phalanges and $10/\mathrm{cm}^2$ in the rest of the hand[24,31]. Each PC was driven by the time-varying skin oscillations $u(\mathbf{x}_m, t)$ and produced a spike train specified via an ordered array $Y_m = \{t_1, t_2, ..., t_Q\}$ of spikes at times t_i, where Q was the number of stimulus-evoked

spikes. Except where otherwise noted, the PC neuron model type for each PC in each assembled population was randomly selected to be one of the four PC neuron model types noted above.

PC entrainment threshold curves

Entrainment threshold curves were constructed to characterize PC frequency sensitivity. Each threshold curve $E_m(f)$ recorded the minimum peak-to-peak skin displacement across the hand evoked by a sinusoidal stimulus (D_{pp}, Eq. 2) necessary to elicit entrainment in PC m across a range of frequencies (20 - $800\,\mathrm{Hz}$). Entrainment was reached when the number of elicited spikes equaled the number of stimulus cycles. The maximum D_{pp} tested was $100\,\mu\mathrm{m}$. In prior literature, threshold curves were determined by placing the stimulating probe placed directly above the hotspot of the terminating neuron[9–13]. In this work, we instead accounted for biomechanical filtering by keeping the contact location constant and constructing threshold curves for PCs distributed throughout the hand.

Preferred frequency was computed as $\arg\min_f\{E_m(f)\}$ and represented the frequency at which the PC was most sensitive. The width of the threshold curve was determined as the full width of the entrainment curve (not necessarily contiguous) at half-minimum and characterized the sensitivity bandwidth of the respective PC.

Correlation analysis

The similarity of different PC entrainment threshold curves was assessed by computing their pairwise correlations, computed as Pearson correlation coefficients, c_{ij}, where i and j index PCs. Subpopulations were designated based on PC location. PC subpopulations P_{mn} were constructed to assess the similarity between curves of PCs at different distances from the contact location. P_{mn} contained PCs located more than m mm but less than n mm from the contact location, where $m < n$. The distances between PCs and the contact location was computed on the 2D hand surface via Djikstra's algorithm. The mean of all possible pairwise correlations between curves in the subpopulation closest to the contact location, P_0, and

curves in another subpopulation, P_{mn}, was calculated as

$$\sigma_{mn} = \frac{1}{MN} \sum_{i=1}^{M} \sum_{j=1}^{N} c_{ij}, \tag{4}$$

where M is the number of PCs in P_0 and N is the number of PCs in P_{mn}. This value was calculated for all $P_{mn} \neq P_0$. When $P_{mn} = P_0$, the mean correlation σ_0 was calculated as

$$\sigma_0 = \frac{2}{M(M-1)} \sum_{i=1}^{M} \sum_{j=i+1}^{M} c_{ij}. \tag{5}$$

PC population encoding efficiency analyses

Efficient encoding hypotheses posit that neural sensory circuitry should minimize redundancy[34–36]. To assess encoding efficiency within PC population responses, the magnitude and timing of PC spiking activity, both of which are involved in tactile encoding[45–47], were analyzed using a diverse set of stimuli based on prior studies of commonly occurring tactile signals[25,26]. The stimulus set consisted of 60 sinusoidal, 117 diharmonic, and 50 bandpass noise input stimuli. Simulation yielded spike timings Y_m for each PC on the hand for each of the 227 stimuli. This procedure was performed for all participants and contact locations.

To assess the redundancy in spiking responses of remotely located PCs, PC subpopulations P_r were constructed containing PCs within r mm of the contact location. As r increased, PCs further from the contact location became included in the subpopulation. Principal component, interspike interval (ISI), and spike train correlation analyses were conducted on the spiking responses of these PC subpopulations as a function of r.

Stimulus set

The stimulus set consisted of sinusoidal, diharmonic, and bandpass noise stimuli presented at various amplitudes (see Supplementary Methods). The sinusoidal stimuli were $100\,\mathrm{ms}$ in duration and were presented at 12 distinct frequencies (50, 75, 100, 150, 200, 250, 300, 400, 500, 600, 700, and $800\,\mathrm{Hz}$) and 5

amplitudes per frequency. The diharmonic stimuli were $100\,\mathrm{ms}$ in duration and comprised 13 frequency pairs (50/100, 50/150, 50/250, 50/500, 50/800, 100/200, 100/300, 100/500, 100/800, 200/400, 200/600, 200/800, and 400/800 Hz) and 9 amplitude combinations per pair. The bandpass noise stimuli were $1000\,\mathrm{ms}$ in duration and comprised 10 distinct frequency bands (50-100, 50-250, 50-500, 50-800, 100-250, 100-500, 100-800, 250-500, 250-800, and 400-800 Hz) and 5 amplitudes per band.

Firing rate analysis

To assess the dimensionality of the magnitude of PC spiking activity, principal component analysis (PCA) was performed on the firing rates for each PC in subpopulation P_r in response to each stimulus. The PC firing rate produced by a given stimulus was calculated by dividing the total number of elicited spikes by the total stimulus duration. This yielded a matrix of firing rates for each subpopulation P_r, where the number of columns was the number of PCs in P_r and the number of rows was the number of stimuli. The data was standardized along the columns (zero-mean and unit standard deviation). PCA was performed to determine the number of principal components that captured at least $99\,\%$ of the variance in the firing rates. The number of principal components can be understood as the number of PCs required to encode the firing rates produced by a population of PCs in response to the entire stimulus set, with higher numbers indicating greater heterogeneity in the firing rates.

Interspike interval analysis

Interspike intervals (ISIs) were computed from the PC spike timings Y_m as $t_{i+1} - t_i,$ where $1 \leq i < Q$, yielding $Q - 1$ ISIs. For a given subpopulation P_r, ISIs were aggregated from all PCs in the subpopulation in response to the whole stimulus set. Probability histograms were computed from the aggregated ISIs, where the sum of all binned values was 1 and the bin width Δt (Fig. 4b, Extended Data Fig. 9). In the main analysis, $\Delta t = 1\,\mathrm{ms}$, as prior research has shown that PCs may encode touch information within spike timing on the order of a millisecond[26]. The information entropy of an ISI histogram $\mathbf{p}$ was calculated as

$$H(\mathbf{p}) = -\sum_{i=1}^{N} \mathbf{p}_i \log_2(\mathbf{p}_i), \tag{6}$$

where N was the number of time bins. This procedure was also performed for individual stimuli in the set (Fig. 4b, Extended Data Fig. 9). Higher ISI entropy values indicated less redundancy within PC population spike timing activity. This analysis did not take into account relative differences in spike times across responses from different PCs.

Spike train correlation analysis

Spike train correlation analyses[48–50] (Fig. 4, Extended Data Fig. 11) were performed by transforming the spike timings Y_m into binned spike train vectors with bin width Δt (Python package elephant[51]). Again, $\Delta t = 1\,\mathrm{ms}$ in the main analysis. We define $\mathbf{s}_m^n$ as the binned spike train produced by PC m in response to stimulus n. Pairwise spike train correlations c_{ij}^n were computed between $\mathbf{s}_i^n$ and $\mathbf{s}_j^n$ (Pearson correlation coefficient). The mean spike train correlation $c(r)$ for subpopulation P_r was calculated as

$$c(r) = \frac{2}{M(M-1)} \sum_{i=1}^{M} \sum_{j=i+1}^{M} \frac{1}{227} \sum_{n=1}^{227} |c_{ij}^n|, \tag{7}$$

where M is the number of PCs in a subpopulation P_r. Lower spike train correlations indicated less redundancy within population spike timing activity. In contrast to the ISI entropy analysis, spike train correlations took into account the relative differences in spike times between different PCs.

References

43. Fradet, C., Manfredi, L. R., Bensmaia, S. & Hayward, V. *Fingertip skin as a linear medium for wave propagation* in *2017 IEEE World Haptics Conference (WHC)* (2017), 507–510.

44. Timmer, J. & König, M. On Generating Power Law Noise. *Astronomy and Astrophysics* **300,** 707–710 (1995).

45. Harvey, M. A., Saal, H. P., Iii, J. F. D. & Bensmaia, S. J. Multiplexing Stimulus Information through Rate and Temporal Codes in Primate Somatosensory Cortex. *PLOS Biology* **11,** e1001558 (2013).

46. Saal, H. P., Harvey, M. A. & Bensmaia, S. J. Rate and timing of cortical responses driven by separate sensory channels. *eLife* (2015).

47. Long, K. H., Lieber, J. D. & Bensmaia, S. J. Texture is encoded in precise temporal spiking patterns in primate somatosensory cortex. *Nature Communications* **13,** 1311 (2022).

48. Bair, W., Zohary, E. & Newsome, W. T. Correlated Firing in Macaque Visual Area MT: Time Scales and Relationship to Behavior. *Journal of Neuroscience* **21,** 1676–1697 (2001).

49. Kohn, A. & Smith, M. A. Stimulus Dependence of Neuronal Correlation in Primary Visual Cortex of the Macaque. *Journal of Neuroscience* **25,** 3661–3673 (2005).

50. Cohen, M. R. & Kohn, A. Measuring and interpreting neuronal correlations. *Nature Neuroscience* **14** (2011).

51. Denker, M., Yegenoglu, A. & Grün, S. *Collaborative HPC-enabled workflows on the HBP Collaboratory using the Elephant framework* in *Neuroinformatics 2018* (2018), P19.

Acknowledgements

We thank Benoit Delhaye for helpful research discussions. We thank Polytec Inc. for the use of the vibrometry system. This work was supported by a Link Foundation Modeling, Simulation, and Training Fellowship (NT), a UCSB Graduate Opportunity Fellowship (NT), Leverhulme Trust research project grant RPG-2022-031 (HPS), and NSF award 1751348 (YV).

Author contributions

NT, GR, HPS, and YV designed the research. BD, YS, and YV collected the vibrometry data. NT, GR, and BD performed the data analysis and research. NT, GR, HPS, and YV wrote the manuscript, and all authors contributed to review and editing.

Competing interests

The authors declare no competing interests.

Additional information

Correspondence and requests for materials should be addressed to Yon Visell (yonvisell@ucsb.edu).